



Effect of HIP post-processing at 850 °C/200 MPa in the fatigue behavior of Ti-6Al-4V alloy fabricated by Selective Laser Melting

J.M. Alegre^{a,*}, A. Díaz^a, R. García^b, L.B. Peral^{a,c}, I.I. Cuesta^a

^a University of Burgos. Escuela Politécnica Superior, Av de Cantabria s/n, 09006 Burgos, Spain

^b HIP Innovation Center, Hiperbaric S.L., C. Condado de Treviño, 6, 09001 Burgos, Spain

^c University of Oviedo, Departamento de Ciencia de los Materiales e Ingeniería Metalúrgica, Escuela Politécnica de Ingeniería de Gijón, Campus de Viesques, 33203 Gijón, Spain

ARTICLE INFO

Keywords:

Ti-6Al-4V
Hot isostatic pressing
Selective Laser Melting
Fatigue behavior
Microstructure

ABSTRACT

Hot Isostatic Pressing (HIP) is a thermomechanical post-processing technique widely used in Additive Manufacturing parts to reduce internal defects, such as entrapped-gas-pores or lack-of-fusion, which have a great influence on the mechanical and fatigue properties of the material. In this paper, the effect of a non-conventional HIP-cycle on the fatigue behavior of a Ti-6Al-4V alloy manufactured by Selective Laser melting (SLM) is studied. The HIP-cycle examined in this study is carried out at pressure of 200 MPa and a temperature of 850 °C for 2 h. Moreover, the cooling process is faster than that obtained from conventional furnace cooling rates, with the aim to limit the microstructural coarsening effects that affect the fatigue behavior. For the study, an extensive experimental fatigue program was carried out which included a first batch of SLM specimens tested under *as-built* conditions, a second batch of SLM specimens subjected to the present HIP process, and a third batch of specimens of a reference wrought processed material obtained by rolling and annealing processes. The microstructure of the material, before and after HIPping, is analyzed and a fractographic analysis is carried out to study the mechanism of crack initiation and its relation to the fatigue behavior. The results show that the present HIP-process allows for very good material densification, a microstructure that shows minimal coarsening effects, and good fatigue properties comparable to the conventional wrought processed material.

1. Introduction

Laser Powder Bed Fusion (LPB-PBF/M) of metals [1,2], also commonly termed as Selective Laser Melting (SLM) is one of the most promising additive manufacturing (AM) techniques widely used for critical components in aerospace, biomedical, and automotive sectors, due to its great versatility for achieving complex geometries and the possibility of working with high added-value materials such as Ti-6Al-4V alloys. However, one of the main problems of AM techniques is the presence of internal defects, a lack-of-fusion or entrapped-gas-pores, which are the main cause of fatigue crack initiation in these components [3,4].

The manufacturing parameters used during the SLM process (hatch laser power, scan speed, layer thickness, scan spacing, preheating temperature, scan strategy, etc.) have a great influence on the internal porosity originated in the material, microstructure, and mechanical properties. Several studies can be found in the literature focused on the

optimization of the manufacturing parameters for the reduction of these internal defects [5-7]. However, although a significant reduction in porosity is achieved by controlling the manufacturing parameters, it is almost impossible to completely avoid the presence of defects in the entire manufactured volume. For this reason, SLM technique applied to critical components is associated with a post-processing stage focused on densifying the material and reducing the number or size of these internal defects.

Hot Isostatic Pressing (HIP) is a widely used thermomechanical postprocessing technique to reduce or eliminate the AM internal defects, such as porosity or lack of fusion, and as consequence improve the mechanical and fatigue properties of critical components. The most important parameters of a HIP-cycle are pressure, temperature and residence time, along with heating and cooling rates. For most materials and applications, the HIP-process also must be carried out in a protective atmosphere, commonly an Argon atmosphere, to prevent oxidation.

The standard HIP-cycle for Ti-6Al-4V alloys manufactured by SLM

* Corresponding author.

E-mail address: jalegre@ubu.es (J.M. Alegre).

<https://doi.org/10.1016/j.ijfatigue.2022.107097>

Received 3 January 2022; Received in revised form 25 May 2022; Accepted 22 June 2022

Available online 25 June 2022

0142-1123/© 2022 The Author(s). Published by Elsevier Ltd. This is an open access article under the CC BY license (<http://creativecommons.org/licenses/by/4.0/>).

consists of heating to a temperature of 900–920 °C and a pressure of around 100–120 MPa, in an Argon atmosphere, and usually followed by furnace cooling [6,8-18]. Typical heating and cooling rates of about 10 °C/min are reported. Some authors have carried out treatments at higher temperature, such as Wu *et al.*, HIPping at 1000 °C / 150 MPa for 1 h [19] or Seifi *et al.* [20] HIPping at 950 °C / 100 MPa for 3 h, and they observe as certain material properties decrease with an increased heat treatment temperature as a consequence of microstructural coarsening effects. This has motivated the study of HIP treatments at higher pressures but lower temperatures combined with rapid cooling to limit these microstructural coarsening effects [21,22].

Microstructural changes during the SLM and HIP processes have a significant effect on the mechanical properties of titanium alloys [23]. Ti-6Al-4V processed by SLM, in the *as-built* conditions, shows a fully martensitic microstructure with a hierarchical acicular morphology of α' martensite [24]. During solidification of the molten metal, columnar prior elongated β -grains grow in the direction of the thermal gradient, and during the cooling of the metal, when the temperature drops below the β -transus ($T_\beta = 995$ °C), phase transformations occur within the $\alpha + \beta$ region. Consequently, fine α -lamellae nucleate and grow in the parent β -grains. This typical microstructure of the SLM *as-built* also contains some intrinsic internal defects, such as lack-of-fusion or entrapped-gas-pores.

For SLM *as-built* parts, the HIP-process is applied at a higher temperature than the martensitic transformation start temperature ($M_s = 800$ °C) and below the β -transus temperature ($T_\beta = 995$ °C), as presented in Fig. 1. In this range of temperatures, the martensitic α' phase transforms into a more stable $\alpha + \beta$ microstructure. For titanium alloys, martensitic transformation produces a very weak distortion and moderate hardening due to the hcp lattice of both of α' and α phases [25]. However, the phase transformation in Ti-6Al-4V strongly depends on the temperature and cooling rates of the HIP-process.

The width of the α plates after heat treatment is depends primarily on the maximum temperature for sub-transus treatments [7]. As a consequence, the HIP-temperature has a great influence on the final thickness of the α -lamellae. The α laths are significantly coarser for higher HIP-process temperatures. The residence time and cooling rate do not have a significant influence for sub-transus treatments, although their effect is more significant the higher the temperature of the process. [26]. In one study, after a HIP treatment at 920 °C for 2 h, α lamellae grew significantly coarser compared to the *as-built* samples, from about 1.0–1.2 μm to approximately double the values after the HIP-process [17,20,27].

Seifi [20] studied the effects of HIPping at 100 MPa for 3 h at 950 °C ± 10 °C in an argon atmosphere followed by furnace cooling. This HIP temperature was slightly higher than the one typically used (e.g. 900–920 °C) but below the β transus temperature. Their results showed a

coarsening of α laths thickness, from about 1.0–1.2 μm to approximately 2.2 μm after the HIP-process, and changes to the toughness and crack growth resistance. Wycisk *et al.* [28] reported that an HIP-process at 920 °C / 100 MPa for 2 h and furnace cooling results in a coarsening of the lamellar microstructure from an α -lamellae thickness of approximately 1 μm to 4 μm and the formation of small amounts of β -phase in between single α -lamellae.

The mechanical and fatigue properties of the Ti-6Al-4V $\alpha + \beta$ alloy are highly influenced by the thermomechanical treatment or heat treatment as a consequence of these microstructural changes. A comprehensive overview of the relationship between the microstructural features and the most important mechanical properties is summarized in Table 1 [23].

Over the last few years, a large number of research papers have been carried out focused on the study of the fatigue properties of Ti-6Al-4V produced by SLM under different processing and post-processing conditions. Table 2 presents a brief summary of some relevant papers that, without claiming to be exhaustive, as it is beyond the scope of this work, shows the current state and future goals.

One of the most referenced works is the one developed by Leuders *et al.* [11]. They carried out an extensive study of the relationship between microstructure, defects and properties, for different conditions including *as-built* states, heat treatments at 800 °C and 1050 °C, and HIPping at 920 °C.

Wycisk *et al.* [28,30] investigated the fatigue performance of Ti-6Al-4V produced by SLM under cyclic tension–tension until 10^7 cycles and tension–compression load until 10^9 cycles for different conditions, including *as-built* and HIPed specimens. In an earlier paper [29], the same authors analysed the fatigue performance of SLM generated parts for different surface conditions, including *as-built* and polished samples. *As-built* non-machined samples showed a poor surface and, as a consequence, a lower fatigue limit about 210 MPa was obtained. Crack initiation occurred at the rough outside surface. The fatigue limit of polished samples was found to be 510 MPa when crack initiated at the surface, but the number of cycles reduced to the order of 10^5 cycles for

Table 1
Influence of microstructure on properties of Ti-6Al-4V. Source: Leyens *et al.* [23].

Fine	Coarse	Property	Lamellar	Equiaxed
+ ↑	– ↓	Strength	– ↓	+ ↑
+ ↑	– ↓	Ductility	– ↓	+ ↑
+ ↑	– ↓	Fatigue crack initiation	– ↓	+ ↑
– ↓	+ ↑	Fatigue crack propagation	+ ↑	– ↓
– ↓	+ ↑	Fracture toughness	+ ↑	– ↓

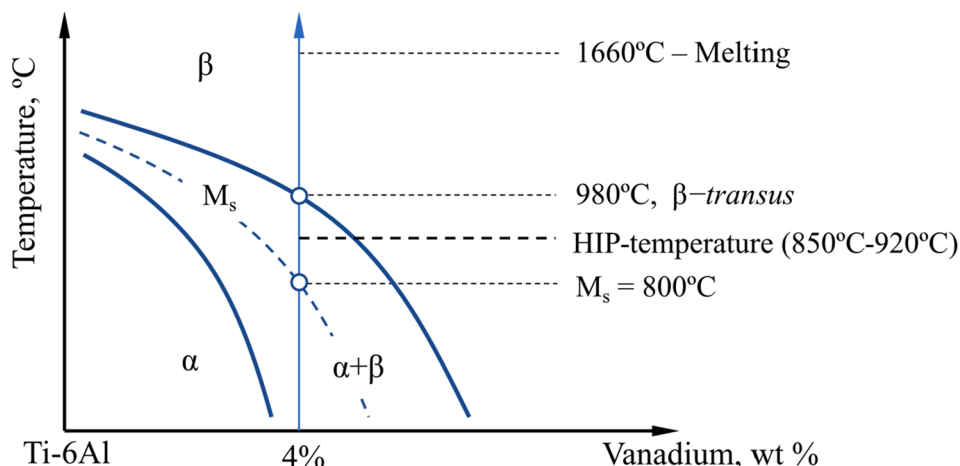


Fig. 1. Schematic pseudo-binary phase diagram of the Ti-6Al-4V.

Table 2
Fatigue properties of SLM Ti-6Al-4V conventionally fabricated and post-treated conditions.

Author [ref.]	Test conditions	YS (MPa)	UTS (MPa)	E(%)	R	f (Hz)	σ_{amp} (MPa)	Run out or failure
Leuders (2013) [11]	As-built	1008	1080	1.6	-1	40	600	27,000
	800 °C / 2 h	962	1040	5	-1	40	600	93,000
	1050 °C / 2 h	798	945	11.6	-1	40	600	290,000
	HIP / 920 °C / 1000 bar / 2 h	912	1005	8.3	-1	40	600	+ 2x10 ⁶
Wycisk (2013)[29,30]	As-built (Ra = 13 µm)	900	1010	7.5	0.1	50	210	+ 10 ⁷
	As-built / machined (Ra = 0.5 µm)	900	1010	7.5	0.1	50	510	10 ⁵ -10 ⁷
Rafi (2013) [31]	As-built / machined	1143	1219	4.89	0.1	50	247,5	+ 10 ⁷
Wycisk (2015) [28]	As-built, SR 650 °C/3h in vacuum / polished	1076	1189	13.6	0.1	50	225	+ 10 ⁷
	HIP 920/1000 bar/2h /polished	907	1022	17.7	0.1	50	306	+ 10 ⁷
	As-built, SR 650 °C/3h in vacuum / polished	1076	1189	13.6	-1	59	350	+ 10 ⁹
	HIP 920/1000 bar/2h /polished	907	1022	17.7	-1	59	575	+ 10 ⁹
Rekedal (2015) [32]	As-built / stress relieved	862	937	-	0.1	60	103,5	+ 10 ⁷
	HIP 899 °C / 102 MPa / 2 h	835	910	-	0.1	60	108	+ 10 ⁷
Gong(2015) [33]	As-built (optimum parameters OP-1)	1098	1237	8.8	0.1	50	157,5	+ 10 ⁷
Xu (2015) [34]	As-built (ELI)	-	1106	11.4	0.1	10	180	+ 10 ⁷
Kasperovich (2015) [6]	As-built	736	1051	11.9	-1	82	600	2.3-5.6 × 10 ³
	As-built / machined	986	1155	10.9	-1	82	600	1.2-2.0 × 10 ⁴
	Annealed 700 °C / 1 h	1051	1115	11.3	-1	82	600	3.0 × 10 ⁴
	Annealed 900 °C / 2 h	908	988	9.5	-1	82	600	3.0 × 10 ⁵
	HIP / 900 °C / 1000 bar / 2 h / machined	885	973	19	-1	82	350	+ 10 ⁷
	As-built + HT 670 °C / 5 h	1022	1092	16.5	-1		343	5 × 10 ⁷
Benedetti(2016)[35]	HIP / 920 °C / 1000 bar / 2 h	850	962	22.5	-1		369	5 × 10 ⁷
	As-built	1015	1090	10	-1	150	220	5 × 10 ⁷
Benedetti(2017)[36]	As-built tribofinished	850	960	14	-1	150	340	5 × 10 ⁷
	As-built electropolished	850	960	14	-1	150	250	5 × 10 ⁷
	HIP / 920 °C / 1000 bar / 2 h	850	960	14	-1	150	370	5 × 10 ⁷
	As-built	1065	1241	6	-1	130	286	+ 10 ⁷
Yan (2018)[37]	HT 900 °C / 2 h / Furnace Cooling	869	945	18	-1	130	337	+ 10 ⁷
	HIP 900 °C / 120 MPa / 2 h	839	941	19	-1	130	374	+ 10 ⁷
	As-built + HT 640 °C / 4 h / polishing	961	1032	2.7	-1	85	288	+ 10 ⁷
Chastand (2018)[38]	As-built	1086	1246	11	-1	60	120	2 × 10 ⁶
	Stress Relief 850 °C / 2 h / air cooling	926	1002	16	-1	60	235	2 × 10 ⁶
	HIP 920 °C / 1000 bar / 2 h	860	960	18	-1	60	200	2 × 10 ⁶
Cutolo (2019) [13]	As-built	1086	1246	11	-1	60	120	2 × 10 ⁶
	Stress Relief 850 °C / 2 h / air cooling	926	1002	16	-1	60	235	2 × 10 ⁶
Mertova (2018)[39]	HIP 920 °C / 1000 bar / 2 h	860	960	18	-1	60	200	2 × 10 ⁶
	As-built / annealed 820 °C-1.5 h / machined	973	1023	9	-1	50	220	+ 10 ⁷
	HIP 920 °C-1000 bar-2 h / machined	-	-	-	-1	50	350	+ 10 ⁷
Roudnicka (2019) [10]	HIP 920 °C-1000 bar-2 h / as deposited	946	1043	13.9	-1	50	230	+ 10 ⁷
	As-built / annealed 820 °C-1.5 h	973	1023	9	-1	50	212	+ 10 ⁷
	HIP 920 °C-1000 bar-2 h / as-deposited	946	1043	13.9	-1	50	222	+ 10 ⁷
Moran (2022) [22]	Standard HIP 920 °C / 100 MPa / 2 h	-	-	-	0.1	10	388	3,4 × 10 ⁴
	Super-beta HIP 1050 °C / 100 MPa / 2 h	-	-	-	0.1	10	388	2 × 10 ⁴
	HIP 800 °C / 200 MPa / 2 h	-	-	-	0.1	10	388	1.5 × 10 ⁶

500 MPa if crack initiation occurred at internal pores. In the latter case, a significant fatigue scatter was observed.

Rekedal [32] studied the effect on fatigue life on flat SLM specimens after a HIP treatment at 899 °C and 102 MPa for 2 h, maintaining the as-built surface conditions. They also compared the effect of a heat treatment at 800 °C for 2 h on the fatigue behaviour. The fatigue strength was very similar for both cases, especially for long lives, showing that the effect of the surface finish is crucial for the fatigue life, and that no significant differences exist between a stress relief heat treatment and a HIP treatment for an as-built condition surface.

Gong *et al.* [33] studied the mechanical and fatigue properties of Ti-6Al-4V samples produced by SLM. Different combinations of process parameters with varying energy density levels and scan speed were utilized to produce the samples. No heat treatment was performed on any of the samples produced in this study. The fatigue limit of SLM samples produced was found to be considerably lower ($\sigma_{max} = 350$ MPa, $R = 0.1$) than values ($\sigma_{max} = 550$ MPa, $R = 0.1$) reported by Rafi *et al.* [31] for SLM samples produced using the same EOS recommended process parameters and the same stress ratio for testing. The difference was attributed to the machined sample surface used by Rafi *et al.*

Xu *et al.* [34] presented an interesting study of the fatigue behavior of SLM Ti-6Al-4V (ELI) specimens, controlling temperatures during the process. Prior to SLM, the powder bed was preheated to 200 °C, and during the process the average temperature maintained in the previously deposited layers was close to 400 °C. Thickness of a lath as a function of the post-heat treatment temperature (all for 2 h) was also

studied. Fatigue testing was performed at two stress levels, 400 and 600 MPa, under load control with an R ratio of 0.1 and a frequency of 10 Hz. The samples for fatigue testing were machined from the as-fabricated SLM Ti-6Al-4V. Fatigue lives above of 2×10^6 are obtained for ultra-fine lamellar structure (with α lath thickness of 0.31 µm) under an applied maximum stress of 400 MPa.

Kasperovich *et al.* [6] also carried out an extensive study of the fatigue properties of SLM Ti-6Al-4V produced samples at different conditions, including as-built specimens, as-built and machined specimens, specimens subjected to heat treatments at 700 °C and 900 °C and HIPed samples at 900 °C / 1000 bar / 2 h. The effect of surface finish in the fatigue behaviour has been widely studied by Benedetti *et al.* [35,36] including a comparison with HIPed specimens using a conventional cycle. Yan *et al.* [37] studied the effect of heat treatment on the phase transformation and mechanical properties of Ti-6Al-4V fabricated by SLM, and analysed the tensile properties for different heat treatments at 800, 900, 920, 950 and 1080 °C, as well as HIPed at 900 °C / 120 MPa / 2 h. They also present fatigue results for as-built conditions, HT at 900 °C and HIP at 900 °C, respectively. Mertova *et al.* [39] and Roudnicka *et al.* [10] also explored the influence of surface machining and postprocessing by HIP on the fatigue properties of SLM produced components.

Chastand *et al.* [38] studied the fatigue behaviour of a SLM processed Ti-6Al-4V specimens, where both a stress relief treatment at 640 °C for 4 h and a HIP treatment at 920 °C / 1020 bar / 2 h are analysed.

Cutolo *et al.* [13] studied the fatigue behaviour using miniaturized samples with a circular cross section of 2.5 mm in diameter. The authors

investigated two different heat treatments for Ti-6Al-4V produced by SLM, namely, stress-relief (SR) and HIP. For SR, the samples were heated at 850 °C for 2 h followed by air cooling, while for HIP the samples were heated at a temperature of 920 °C at a pressure of 1000 bar for 2 h. All the samples were tested in as-built surface conditions. The poor fatigue property of as-built samples was attributed to the presence of high residual stress levels generated during the SLM production process and the brittle α' martensitic microstructure obtained in these specimens. SR produces substantial improvement of Ti-6Al-4V fatigue properties, reaching values similar to other author for as-built conditions with optimized fabrication parameters. The improvement of the SR heat treatment is also attributed to the microstructure refinement of the α' martensitic microstructure into a fine lamellar $\alpha + \beta$.

Fatemi et al. [40] present an overview of some recent experimental studies on Ti-6Al-4V considering various processing and loading direction effects. In particular, they collect the effect of residual stresses, surface finish, specimen geometry and size, layer orientation during fabrication, heat treatments including HIP. They conclude that residual stresses can be eliminated or significantly reduced by using the appropriate manufacturing process parameters, as well as with post-fabrication heat treatment processes. Moreover, experimental results after HIP treatment show similar performance to a wrought processed material. However, they also claimed that the beneficial effect of HIP treatment can only be observed after surface machining, since the rough surface of as-built HIP specimens is responsible for shortening the fatigue life, especially in the HCF regime.

A large variability in the fatigue behavior of Ti-6Al-4V produced by SLM can be observed among the different studies that have been published in recent years. These great differences can be attributed to the different factors that greatly influence fatigue behaviour of the fabricated part, such as the surface finish, the manufacturing parameters, the stress relief treatments, the load level during the test (R value), or the applied HIP treatment, for example. All these influencing conditions, together with the different microstructures attained, make it very difficult to accomplish a realistic comparison between different authors.

One of the difficulties in comparing fatigue results from different authors arises from the effect of the mean stress itself. Most of the studies to date are carried out for values of $R = -1$ and less frequently for values of $R = 0.1$. In this sense, some authors have established a suitable way to consider the effect of the mean stress in this material. Benedetti et al. [4] proposes the Smith-Watson-Topper model [41] or the one included in the FKM Guide [42] as adequate to compare results obtained with different R values. In addition, a suitable model has also been proposed by Li et al. [43] in which fatigue life could be discussed with respect to an effective stress value σ_{eff} that normalizes differing R values according to:

$$\sigma_{eff} = \sigma_{max} \left(\frac{1-R}{2} \right)^{0.28} \quad (1)$$

where σ_{max} is the actual maximum value of the applied stress during a fatigue load cycle at a given R value. The value of the exponent has been validated by examining fatigue data for traditionally processed Ti-6Al-4V, in the range $R = -0.5$ to $R = 0.5$ [43].

Therefore, the fatigue behavior of Ti-6Al-4V manufactured by SLM is conditioned, among other things, by several features related to the presence of internal defects and surface finish and by the microstructural changes originated during the thermomechanical treatments. When the presence of defects is significant (*as-built* condition or non-machined surfaces) the fatigue strength is conditioned by the size of these defects or the poor surface finish, which become the initiators of the fatigue. However, when the material is treated with a thermo-mechanical process such as HIP, a reduction or elimination of these internal defects is achieved, and from that moment on the fatigue resistance of the material becomes conditioned by microstructural features. It is therefore important to ensure that the HIP process achieves a microstructure which allows the best possible fatigue properties to be obtained.

However, the HIP process only exhibits benefits on the fatigue life of the part when it is accompanied by surface machining, otherwise fatigue is still conditioned by surface defects intrinsic to the poor surface finish of SLM techniques.

Studies on the possible beneficial effects of reducing HIP temperature while increasing pressure are scarce, as previously reviewed. However, the work of Moran et al. [22] must be mentioned as a comprehensive comparison between a standard HIP, i.e. at 920 °C and 100 MPa as recommended by the ASTM F2924, and two alternative cycles: a super-Beta HIP at 1050 °C and 100 MPa in which fatigue behaviour was considerably worse due to the α -grain coarsening, and a low-temperature high-pressure HIP (LTHP-HIP) at 800 °C and 200 MPa. This LTHP-HIP was demonstrated to minimize microstructure coarsening and resulted in the best fatigue performance. Despite some authors [21,22] claim that the size and shape of defects are not expected to control high cycle fatigue, it is clear that a decrease in defect population will reduce fatigue initiation sites. Therefore, the present work tries to shed light into the relationship between microstructure, defects and fatigue life after a low-temperature high-pressure HIP process. In this paper, the fatigue behavior of a Ti-6Al-4V Grade 5 alloy manufactured by SLM and subjected to a HIP treatment at 850 °C and 200 MPa for 2 h is studied. Special emphasis is given to the microstructural aspects, before and after the HIP process, as well as their relationship with the crack initiation mechanisms.

2. Materials and methods

The material used in this research is Ti-6Al-4V Grade 5 alloy. The specimens for this study were made using an SLM device (EOS M280 parameters Ti-6Al-4V) in a protective atmosphere of argon. The Ti-6Al-4V powders used are designated as EOS Titanium Ti64, formed by spherical particles with a size distribution between 27.79 μm (d10) and 54.45 μm (d90) and an average particle diameter of 38.18 μm (d50) according to ISO 13320. Typical SLM parameters for the Ti-6Al-4V alloy were used in this study to make the specimens. The laser power and the scan velocity were 400 W and 150 mm/s, respectively, and the platform temperature was approximately 200 °C. A hatching spacing of 120 μm and a layer thickness of 60 μm were used.

Uniaxial standard tensile specimens were machined from round bars that were previously obtained through SLM in a vertical built direction and processed by HIP. Tensile tests were conducted on cylindrical specimens and tested according to ASTM E8 [44]. Small-Size specimens proportional to standard, with 6 mm in diameter were used. Two specimens were tested for each condition. Table 3 provides a summary of the tensile test properties obtained.

An extensive experimental fatigue program was carried out which included three different set-ups: (a) a first batch of SLM specimens under *as-built* conditions, (b) a second batch of SLM specimens subjected to the present HIP process, and (3) a third batch of specimens of a reference material obtained from a bar of diameter 30 mm, wrought processed and annealed according to ASTM B348-13.

All specimens were machined and finished to final geometry after the heat treatment. Surface roughness has been checked after machining and R_a values range between 0.61 and 0.88 μm for all samples. The focus of the present work is put on the effects of defects produced by SLM, so

Table 3
Mechanical properties of the materials analysed in this study.

Material	Offset yield strength, $R_{p0.2}$ (MPa)	Tensile Strength, R_m (MPa)	Elongation at break (%)	Vickers hardness
SLM as built	1090	1297	11.2	362
SLM + HIP	945	1055	13.2	332
Wrought processed material	894	966	19.5	320

the influence of the surface finish before machining is not analysed. The main dimensions of the fatigue specimens are presented in Fig. 2. Fatigue behavior is characterised through constant amplitude tests under tension–tension ($R = 0.1$) at a frequency of 15 Hz and at a temperature of 20 °C. Fatigue tests were carried out on a servo-hydraulic test machine MTS-810. Failure criteria was established as specimen separation or test run-out at 8 million (8×10^6) cycles.

For the metallographic analysis, Kroll’s reagent (100 mL distilled water, 2 mL HF & 4 mL HNO_3) was used to reveal the microstructure of wet ground and polished samples.

Scanning electron microscopy (SEM) was performed by using a high-resolution field-emission SEM JEOL JSM-6460LV (R&D Center at University of Burgos, Spain) operated at 20 kV. Optical microscope used for metallographic analysis was an inverted microscope Leica DMi8 M.

The HIP treatment was applied in the HIP Innovation Center of the company Hiperbaric (Spain). The HIP-cycle was carried out in an Argon environment, at a sub β -*transus* temperature of 850 ± 3 °C and at a pressure of 200 MPa. The residence time was 120 min. The heating rate was 10–15 °C/min, and the cooling rate was conducted by means of a fast-cooling technology, which quickly decreases the temperature from 850 °C to 300 °C. The HIP-cycle parameters are shown in Fig. 3. The cooling rate inside the vessel during the HIP-cycle is shown in the Fig. 4, which shows the thermo-mechanical process to which the material inside the processing chamber was subjected. The average cooling rate for a temperature between 850 °C and 600 °C was -138 °C/min (similar to forced air cooling). Subsequently, for a temperature of 600 °C to 400 °C, the average cooling rate was approximately -67 °C/min (similar to air cooling). An image of the HIP equipment used in this research is shown in Fig. 5.

Hiperbaric Fast Cooling technology uses a series of technical improvements in HIP equipment allowing to extract heat from the inner of the furnace at an evenly fast rate. Some cooling channels close to the vessel’s liner, combined with a heat exchanger, allow the inner heat extraction. The Fast Cooling feature employs a series of valves and a fan to control the gas flows and achieve an even mixture of cooled gas with the hot gas inside the furnace. The inner hot gas is looped and mixed with an outer cold gas loop introduced and controlled through a series of valves. The gas can escape through an upper path guided to the top plug’s heat exchanger and then cool down by the vessel, where the heat is removed. A scheme of this process is also presented in Fig. 5.

3. Results and discussion

3.1. Microstructure

The microstructure of the different conditions studied in this research are presented in Fig. 6. The microstructure of the *as-built* conditions (Fig. 6(a)) and sub β -*transus* HIP treatment (Fig. 6(b)) consist of α laths arranged in a basketweave type pattern. The obtained microstructure is very similar to the one obtained from Vrancken *et al.* [7], for a Ti-6Al-4V alloy fabricated by SLM and subjected to a heat treatment at 850 °C followed by air cooling.

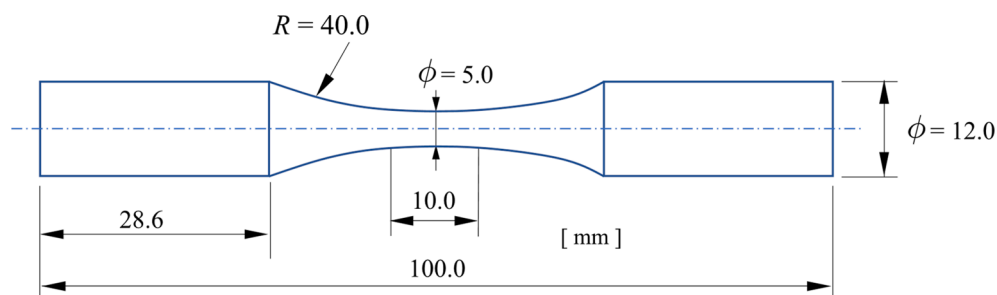


Fig. 2. Fatigue specimen geometry (dimensions in mm).

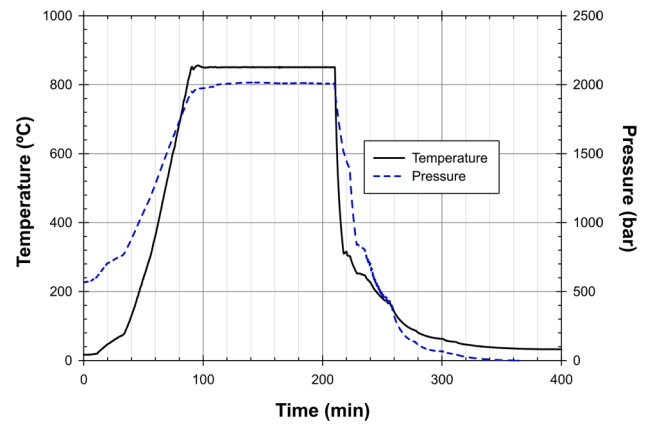


Fig. 3. HIP-cycle carried out in present research.

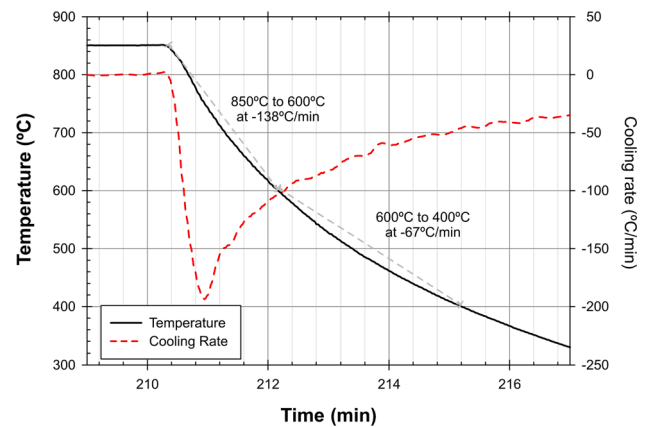


Fig. 4. Detail of the fast cooling stage of the HIP-process.

The α thickness has been measured using the Leica Analysis Software with the module Grain Expert. Images at 50x have been analysed over a region containing 10,000 grains, approximately, considering the same sensitivity and bright threshold for all the analyses. Grain thickness distribution is shown in the histograms in Fig. 7 with the corresponding average and standard deviation values. A slight increase in the average α thickness, from 1.14 to 1.27 μm , is observed after HIP post-processing at 850 °C / 200 MPa for 2 h, but the grain growth is very limited due to the moderate HIP temperature and the fast-cooling process shown in Fig. 5. It can be observed in Fig. 7 how the fraction of grains between 0.0 and 1.0 μm is reduced in the SLM + HIP sample in comparison with the SLM “as-built” condition, whereas the number of grains between 1.0 and 2.0 μm increases after HIP.

The reference wrought processed material, shown in Fig. 6 (c), consists of Ti-6Al-4V equiaxed primary α grains with a main size of 5.92 μm and grain boundaries of β phase. The material was annealed at a

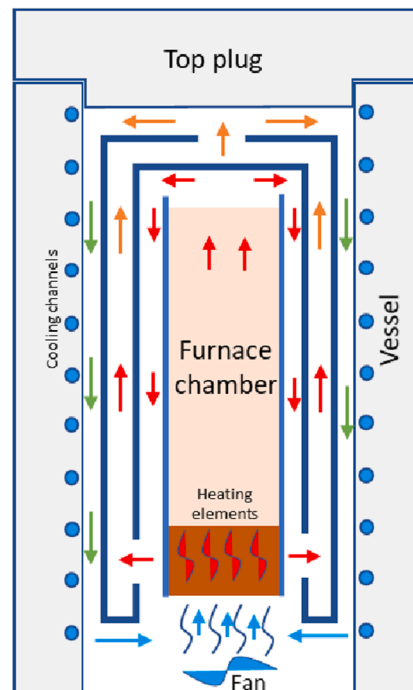


Fig. 5. HIP-equipment at the HIP Innovation Center, Hiperbaric (Spain).

temperature of 750 °C for 90 min. This microstructure results in a good combination of properties, including moderate strength and good ductility, fatigue, toughness and crack growth properties. This heat treatment should result in a totally residual stress-free component [45]. Previous studies indicate that lamellar microstructure exhibits lower strength, lower ductility, and better fatigue propagation resistance compared with equiaxed microstructure. Equiaxed microstructure provides better fatigue initiation resistance but poorer propagation resistance than lamellar microstructure [23,46].

3.2. Fatigue results

Fatigue tests have been conducted on the three batches of (a) SLM *as-built* specimens, (b) the SLM + HIP-treated specimens, and (c) the

reference wrought processed material. The constant amplitude stress levels were applied under tension–tension ($R = 0.1$) at a frequency of 15 Hz. The main results and the tests conditions are collected in Tables 3 and 4 respectively, showing the alternate stress for $R = 0.1$, the number of cycles until failure, the observed fatigue crack initiation mechanism, the initiation site defined as the distance from the center of the defect to the outer surface (in μm), and the defect size initiating the crack. Moreover, the comparative S-N curve including the complete set of results for the different batches is shown in Fig. 8. As expected, the fatigue behavior of the material processed by SLM in the *as-built* condition is much worse than the fatigue behavior of the SLM + HIP processed specimens (see Table 5).

In order to assess the effectiveness of the present HIP cycle, the obtained S-N curve is compared with other results from literature in Fig. 9,

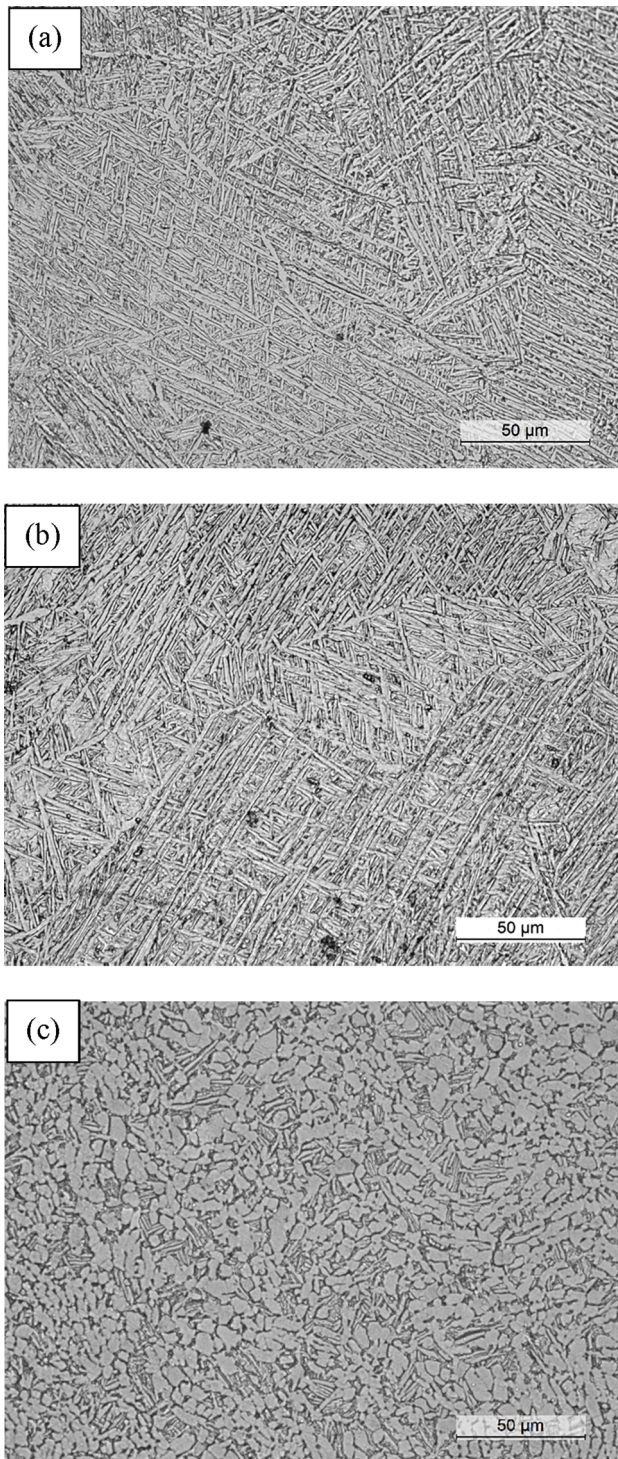


Fig. 6. Microstructure of the three conditions analyzed in this study: (a) SLM as-built, (b) post-processed material, SLM + HIPped at 200 MPa / 850 °C for 2 h, and (c) reference wrought processed material.

where stress values are normalised using the effective stress previously defined in equation (1). It can be observed that the low-temperature high-pressure HIP processes, 850 °C and 200 MPa here and 800 °C and 200 MPa in Moran *et al.* [22], result in a better fatigue response in comparison with the conventional HIP cycle of 100 MPa and 900 °C or 920 °C applied by Kasperovich *et al.* [6] and Mertova *et al.* [39], respectively. Therefore, the beneficial effect of temperature reduction is patent in the shift of fatigue behaviour as a function of temperature; the

fitted curves in this HCF range are ordered, from top to bottom, in the following order: 800 °C [22], 850 °C, 900 °C [6] and 920 °C [39]. However, results from Kasperovich *et al.* [6] for the same HIP cycle in samples with the as-built surface demonstrate that the improvement in fatigue behaviour is only clear in machined surfaces.

Similarly, a comparison between different sample conditions is carried out in Fig. 10 with all the present results, i.e. fatigue curves for the wrought material, for the as-built SLM state and for a LTHP HIP cycle, and with results from literature. All tests collected in that Figure were performed at $R = 0.1$ and thus stress normalization is not required. Despite the difficult data classification, three bands are defined to approximately assess the influence of SLM, surface machining, HIP post-processing and stress relieve. As expected, the worst fatigue response occurs for samples with the as-built rough surface typical of SLM, as obtained by Wycisk *et al.* [30]; the same authors found a clear improvement after machining or polishing the surface. SLM samples in as-built conditions and with machined surfaces are gathered in the middle band in Fig. 10, including results from Wycisk *et al.* [30] and Rafi *et al.* [31]. It must be highlighted that results from Rekedal [32] for non-machined surface showed a better fatigue resistance after a stress relief treatment of 800 °C during 4 h and also lie in that middle band despite a rough sample surface. Tests for the as-built and machined state in the present work resulted in a better fatigue behaviour than other works [30,31], as shown in Fig. 10; this is attributed to the relatively small size of defects and to the moderate residual stress that was produced during SLM. Finally, an upper band with fatigue resistance above 350 MPa can be defined to comprise the present results for a LTHP HIP and data from Moran *et al.* [22], and also the fatigue curve corresponding to the reference wrought material, demonstrating the recovery effect of HIP for fatigue properties.

An analysis of the fracture surface has been conducted with the aim of identifying the fatigue initiation mechanism for all conditions tested. For SLM under *as-built* conditions, the fatigue crack initiates from internal defects such as lack-of-fusion or porosity. A representative example of these internal defects is presented in Fig. 11. The maximum in-plane dimension of lack-of-fusion defects initiating the fatigue is collected in Table 3, with a value between 100 and 200 μm. The defects are irregular in size and shape, and so the $\sqrt{\text{area}}$ parameter (square root of the initial defect projected crack area) can be calculated, because according to the Murakami model [47] this parameter can be considered as the characteristic dimension for the evaluation of the effects of defects of various sizes and shapes on fatigue strength. The mean value of the $\sqrt{\text{area}}$ parameter is equal to 74.15 ± 16.83 μm. The position of defects does not follow any noticeable pattern, occurring at different locations along the radius of the specimen. All defects are internal or near the surface, but any failure is initiated at the outer surface of the specimen. According to the theory of extremes of Murakami and co-workers [48], when the defects become the origin of the fatigue failure, the initiation occurs at the largest defect or inhomogeneity that is present in the volume. As a consequence, the initiation defect represents the largest defect size within the control volume for each specimen. The SLM *as-built* condition tends towards a fatigue limit lower than 275 MPa, as shown in Fig. 8.

The fatigue crack initiation for the SLM + HIP treated specimens exhibits a predominant fatigue initiation mechanism related to microstructural features itself, with no failures detected from internal defects such as lack of fusion or pores. This suggests that a good densification of the material using the current HIP-cycle at 850 °C and 200 MPa for 2 h is achieved, and that the current HIP-cycle can be considered as an effective thermomechanical treatment for the reduction or even elimination of internal defects in this material processed by SLM. Assuming the theory of extremes by Murakami, which postulates that the crack initiates from the largest defect present in the control volume, it can be ensured that lack-of-fusion defects are mostly sealed applying this HIP-cycle. In any case, if some internal defects are not completely

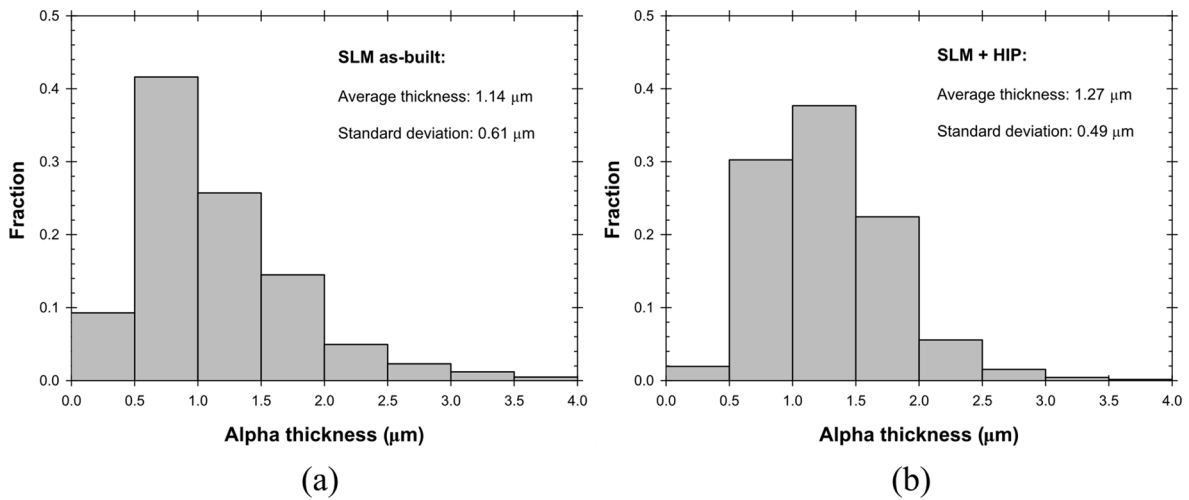


Fig. 7. Distribution of α -lath thickness: (a) SLM as-built, (b) post-processed material (SLM + HIP).

Table 4

Fatigue test results summary for SLM as-built conditions. Initiation mechanism: lack-of-fusion (LOF), Gas pore (GP). Initiation site: distance from the defects to the specimen outer surface (μm), 0 indicates initiation at the surface.

σ_a (MPa)	Number of cycles	Initiation mechanism	Maximum defect size (μm)	Initiation site (μm)	Defect size parameter, $\sqrt{\text{area}}$ (μm)
400	79,044	GP	40	430	32.9
400	85,392	LOF	120	855	81.1
340	350,084	LOF	205	1650	77.3
340	267,173	LOF	142	165	76.9
340	617,908	LOF	139	646	79.6
311	321,300	LOF	188	1393	91.2
311	392,718	LOF	137	1707	72.6
311	1,726,030	LOF	101	219	69.3
300	2,086,518	LOF	143	256	86.5

Table 5

Fatigue result summary for SLM + HIP process. Initiation mechanism: microstructural facets (MF), Surface marks (SM). Initiation site: distance from the defects to the specimen outer surface (μm), 0 indicates initiation at the surface.

σ_a (MPa)	Number of cycles	Initiation mechanism	Initiation site (μm)
450	5050	MF	0
450	6014	MF	0
425	13,434	MF	0
425	15,622	MF	0
400	17,054	MF	0
400	27,810	SM + MF	0
390	62,380	MF	0
380	91,032	MF	0
380	797,518	MF	400
370	53,515	SM + MF	0
370	65,486	MF	0
370	284,228	SM	0
370	1,365,710	MF	175
370	2,035,458	MF	40
370	2,048,848	MF	350
365	1,580,655	MF	50
365	2,299,893	MF	650
360	1,803,180	MF	0
360	1,005,299	MF	0
360	2,756,707	MF	850
360	2,655,960	MF	400
355	>8000000	run-out	-

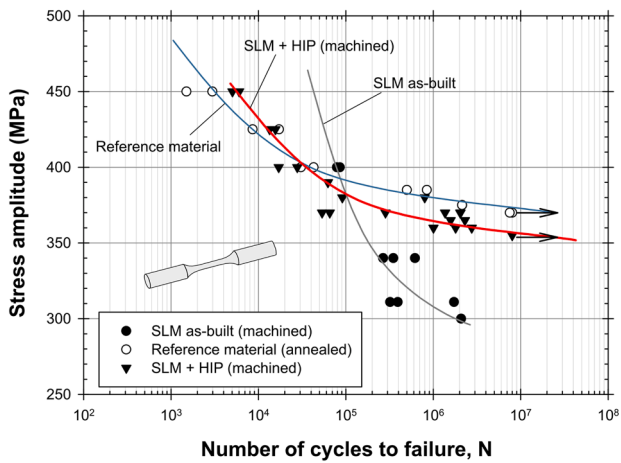


Fig. 8. Fatigue tests results for the three studied conditions: as-built SLM, SLM + HIP, reference wrought material.

eliminated, their small size after HIP does not lead to fatigue crack initiation sites, which suggests the existence of a minimum defect size that competes with microstructural features as the initiating origin of a fatigue crack.

The mechanism of fatigue crack initiation in the SLM $\alpha + \beta$ titanium alloys is well known and reported in detail by many authors [49-53] and is related to the facet formation in alpha phase. The crack initiation

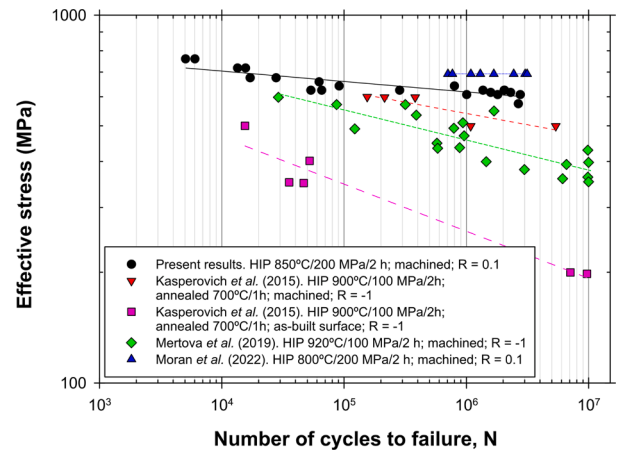


Fig. 9. Comparison of present results with different HIP cycles from literature. Results are plotted in terms of an effective stress to account for R effects.

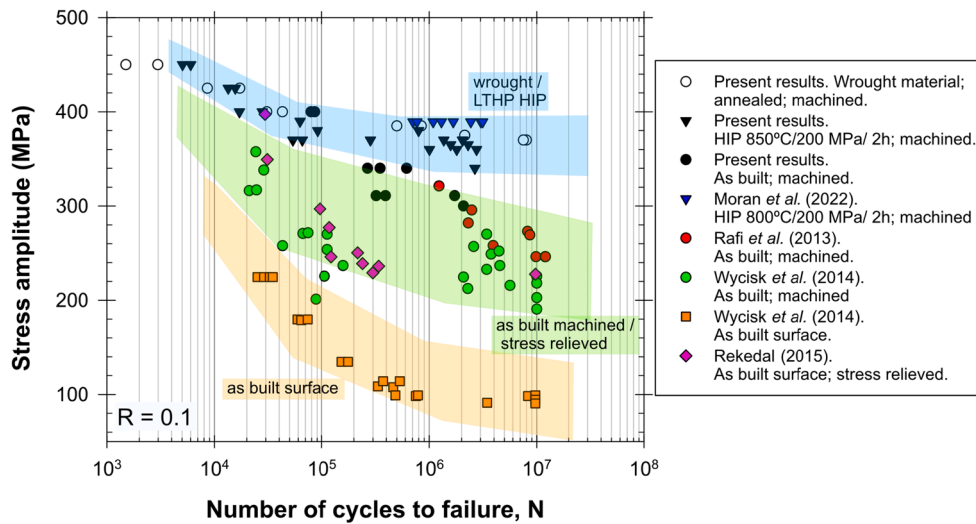


Fig. 10. Comparison of fatigue curves between different conditions, including present results and results from literature.

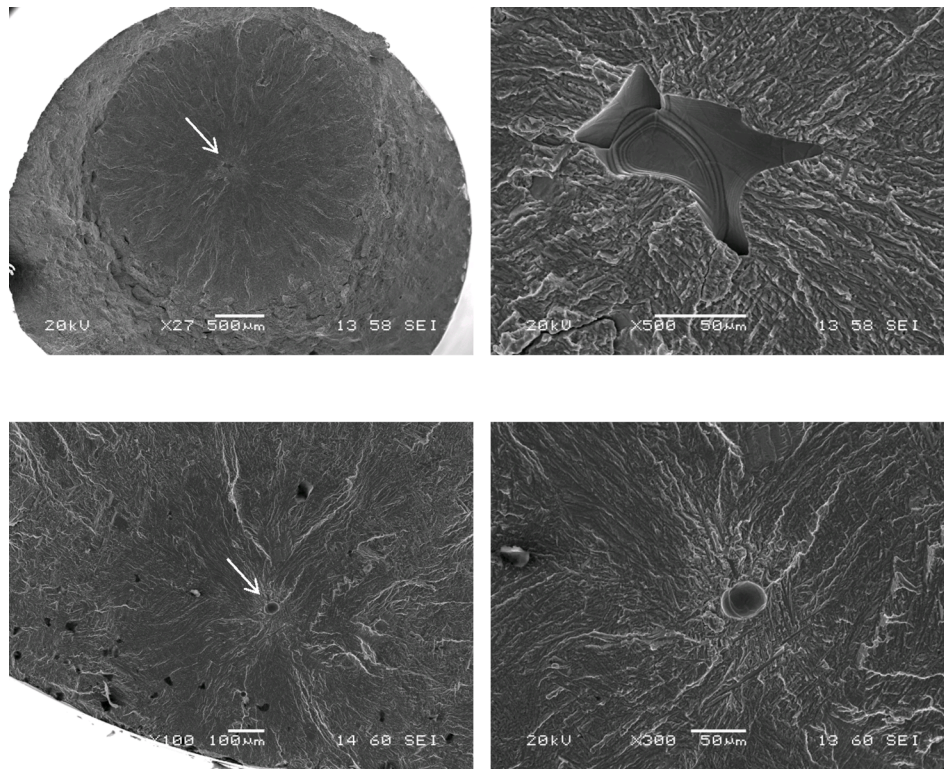


Fig. 11. Fatigue fracture surfaces and crack initiation sites: (a) From an internal “lack-of-fusion” defect type: SLM as-built; (b) From an internal “entrapped-gas-pore” defect type: SLM as-built.

mechanism in these specimens presents a characteristic pattern as shown in Fig. 13, formed by a set of flat facets at the initiation site. The facet size and shape match those corresponding to the α laths, and they present a quasi-cleavage appearance. These fractured α laths or facets are separated by other α lath fractures, but with a more ductile fracture appearance.

Numerous authors have studied the necessary conditions for the formation of a facet in the α phase of the Ti-6Al-4V alloy, as a consequence of the reduced slip planes and the anisotropy of the hcp lattice [53-56]. A theory proposed by Bache [57], which is outlined in Fig. 12. a), is commonly accepted and argues that a “weak grain” is one that is favourably oriented for slip (prismatic or pyramidal planes), and a

“strong grain” has its basal plane perpendicular to the load axis. The conveniently oriented weak grain (1) generates a dislocation pile-up at the boundary with the neighbouring strong grain (2) which has its basal plane perpendicular to the load. The formation of facets is thus generated by the pile-up causing a combination of shear and tensile stresses on the basal plane of the strong grain.

The created facet generates a strong stress concentration in the area that could induce a ductile fracture form neighbouring weak grains or, depending on their orientation, through the ductile grain boundary (β phase) [49,53].

In some cases, there is not any strong grain adjacent to the weak grain, as shown in Fig. 12.b). The facet formation mechanism proposed

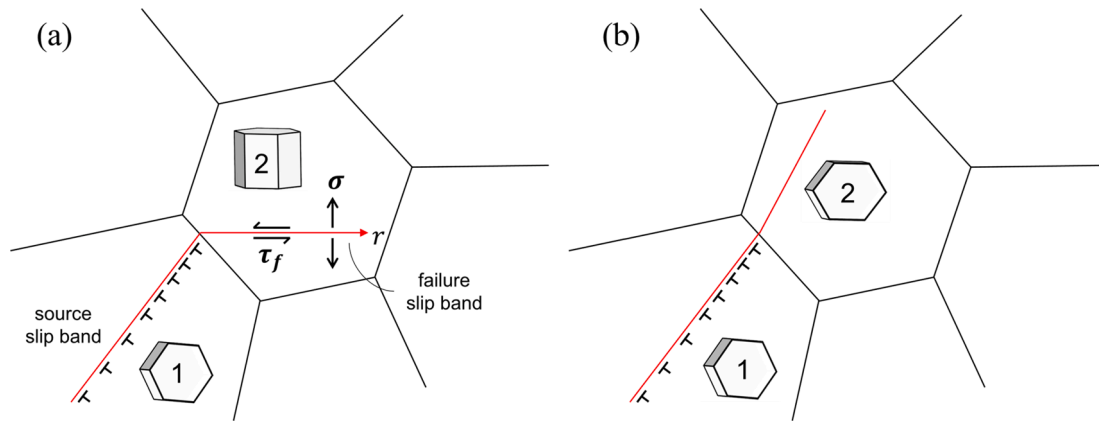


Fig. 12. Facet formation mechanism in α (hcp) titanium grains. Scheme . adapted from [16,18]

by Everaerts [55] also involves a dislocation pile-up origin in the grain (1), but in this case it is caused by the presence of a neighbouring weak grain (2) that induces the facet formation in the grain (1) and then the crack can propagate with a ductile behaviour in the grain (2). This type of mechanism would present inclined facets with respect to the tensile axis, which is observed in the mechanism of the reference material that presents an equiaxial microstructure. These facets are formed from the equiaxial α phase in a perpendicular direction or with a certain inclination with respect to the applied axial stress, as shown in Fig. 14 which indicates that the combination of both mechanisms might operate depending on the orientations of the α phase (see Fig. 14.).

The reduction or elimination of pores and the modification of microstructure in HIPped specimens significantly increases the fatigue limit of material up to 360 MPa, extending the period of fatigue crack initiation. In general, the specimens subjected to the HIP process exhibit

a fatigue behavior slightly worse than the reference wrought material and show a higher scatter in the fatigue life.

For the reference wrought material and for short lives ($<10^6$), the fracture typically initiates at the surface or near the surface, from clusters of facets formed in the α -phase matrix. The facets are simple fractures of α grains in an inclined direction from the fatigue plane and related to the slip and cleavage planes systems in Ti alloys [53,56]. For low stress levels and long lives ($>10^6$ cycles) the fatigue origin is internal, also forming a light area around clusters of facets of α -phase fractures. As already mentioned, these facets are formed in slanted directions with respect to the axial applied stress, as shown in Fig. 14.

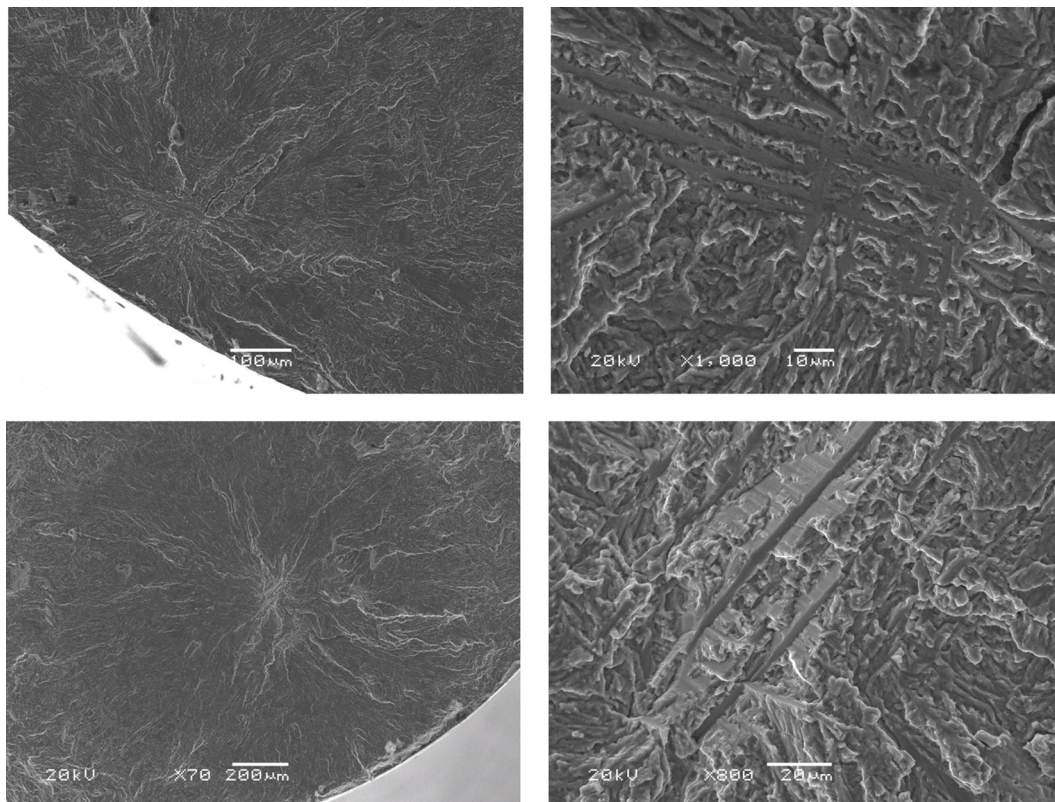


Fig. 13. Some examples of fatigue crack initiation forming fractures of α -phase laths (scratches) and $\alpha + \beta$ interface decohesion (facets), SLM + HIP.

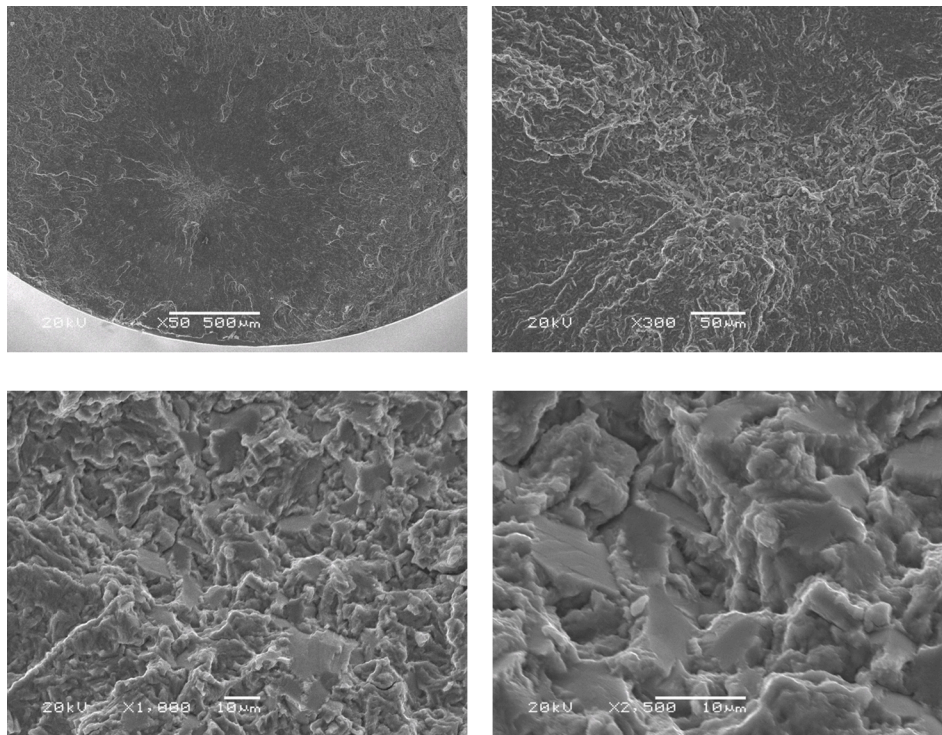


Fig. 14. Typical fracture appearance surrounding an internal fatigue initiation site, at different magnifications.

4. Conclusions

In the present investigation, the fatigue behavior of a Ti-6Al-4V alloy manufactured by SLM and subjected to a HIP treatment at 850 °C and 200 MPa for 2 h has been studied. The specimens were tested in *as-built* conditions and after HIP post-treatment conditions. Moreover, an annealed wrought processed condition was also studied for comparison as representative of the conventionally processed material. The microstructural features related to the origins of the fatigue are studied by subsequent fractography using SEM. The following conclusions can be drawn:

1. The fatigue behavior of additively manufactured Ti-6Al-4V shows two distinct failure modes, i.e. surface fatigue crack initiation and internal fatigue crack initiation. Crack initiation at the outer surface is mainly related to fatigue at low fatigue cycle and high stresses, while internal crack initiation appears for long life ($>10^6$ cycles) and lower stresses.
2. For SLM *as-built* specimens, the fatigue crack initiates from internal defects classified as lack-of-fusion or entrapped-gas-porosity. These defects are irregular in size and shape, exhibiting a maximum length of about 200 μm and a $\sqrt{\text{area}}$ parameter of about 75 μm.
3. For the HIP-treated SLM specimens, the absence of failures initiated from lack-of-fusion or pores indicates a good densification of the material using the current HIP-cycle at 850 °C and 200 MPa for 2 h. In addition, the size of the α -phase slabs does not experience any appreciable thickening after the HIP treatment at 850 °C, which represents an appropriate feature for improving the fatigue life of the material.
4. For the HIP-treated SLM specimens, the fatigue crack is mainly initiated at the $\alpha + \beta$ interfaces forming light areas associated with decohesion of the α -phase slabs (facets). For most specimens, this decohesion of the α -phase facets is accompanied by fractures of the α -phase laths in the form of scratch-like marks on the fracture surface.

5. The fatigue behavior of the SLM + HIP material significantly improves the behavior of the SLM *as-built* material, reaching values similar to those obtained from the reference wrought processed material.

Declaration of Competing Interest

The authors declare that they have no known competing financial interests or personal relationships that could have appeared to influence the work reported in this paper.

Acknowledgements

The authors gratefully acknowledge financial support from the Junta de Castilla y Leon (Spain) through grant BU-002-P20, co-financed by FEDER funds.

References

- [1] ISO - ISO/ASTM 52911-1:2019 - Additive manufacturing — Design — Part 1: Laser-based powder bed fusion of metals; n.d. <https://www.iso.org/standard/72951.html> (accessed May 3, 2022).
- [2] ASTM F2924-14(2021) -Standard Specification for Additive Manufacturing Titanium-6 Aluminum-4 Vanadium with Powder Bed Fusion; n.d. <https://www.astm.org/f2924-14r21.html> (accessed May 13, 2022).
- [3] Hu YN, Wu SC, Withers PJ, Zhang J, Bao HYX, Fu YN, et al. The effect of manufacturing defects on the fatigue life of selective laser melted Ti-6Al-4V structures. *Mater Des* 2020;192:108708.
- [4] Benedetti M, Fontanari V, Bandini M, Zanini F, Carmignato S. Low- and high-cycle fatigue resistance of Ti-6Al-4V ELI additively manufactured via selective laser melting: Mean stress and defect sensitivity. *Int J Fatigue* 2018;107:96–109. <https://doi.org/10.1016/j.ijfatigue.2017.10.021>.
- [5] Song B, Dong SJ, Zhang BC, Liao HL, Coddet C. Effects of processing parameters on microstructure and mechanical property of selective laser melted Ti6Al4V. *Mater Des* 2012;35:120–5. <https://doi.org/10.1016/j.matdes.2011.09.051>.
- [6] Kasperovich G, Hausmann J. Improvement of fatigue resistance and ductility of TiAl6V4 processed by selective laser melting. *J Mater Process Technol* 2015;220:202–14. <https://doi.org/10.1016/j.jmatprotec.2015.01.025>.
- [7] Vrancken B, Thijs L, Kruth JP, Van Humbeeck J. Heat treatment of Ti6Al4V produced by Selective Laser Melting: Microstructure and mechanical properties. *J Alloys Compd* 2012;541:177–85. <https://doi.org/10.1016/j.jallcom.2012.07.022>.

- [8] Qiu C, Adkins NJE, Attallah MM. Microstructure and tensile properties of selectively laser-melted and of HIPed laser-melted Ti-6Al-4V. *Mater Sci Eng A* 2013;578:230–9. <https://doi.org/10.1016/j.msea.2013.04.099>.
- [9] Zhou B, Zhou J, Li H, Lin F. A study of the microstructures and mechanical properties of Ti6Al4V fabricated by SLM under vacuum. *Mater Sci Eng A* 2018;724:1–10. <https://doi.org/10.1016/j.msea.2018.03.021>.
- [10] Roudnicka M, Mertova K, Vojtech D. Influence of hot isostatic pressing on mechanical response of as-built SLM titanium alloy. *IOP Conf Ser Mater Sci Eng* 2019;629(1):012034.
- [11] Leuders S, Thöne M, Riemer A, Niendorf T, Tröster T, Richard HA, et al. On the mechanical behaviour of titanium alloy TiAl6V4 manufactured by selective laser melting: Fatigue resistance and crack growth performance. *Int J Fatigue* 2013;48:300–7. <https://doi.org/10.1016/j.ijfatigue.2012.11.011>.
- [12] Eshawish N, Malinov S, Sha W, Walls P. Microstructure and Mechanical Properties of Ti-6Al-4V Manufactured by Selective Laser Melting after Stress Relieving, Hot Isostatic Pressing Treatment, and Post-Heat Treatment. *J Mater Eng Perform* 2021;30:5290–6. <https://doi.org/10.1007/s11665-021-05753-w>.
- [13] Cutolo A, Elangswaran C, de Formanoir C, Muralidharan GK, Van Hooreweder B. Effect of Heat Treatments on Fatigue Properties of Ti-6Al-4V and 316L Produced by Laser Powder Bed Fusion in As-Built Surface Condition. *Miner Met Mater Ser* (2019) 395–405. https://doi.org/10.1007/978-3-030-05861-6_36/FIGURES/5.
- [14] Wycisk E, Siddique S, Herzog D, Walther F, Emmelmann C. Fatigue performance of laser additive manufactured Ti-6Al-4V in very high cycle fatigue regime up to 10⁹ cycles. *Front Mater* 2015;2:2–9. <https://doi.org/10.3389/fmats.2015.00072>.
- [15] Jamshidi P, Aristizabal M, Kong W, Villapun V, Cox SC, Grover LM, Attallah MM. Selective Laser Melting of Ti-6Al-4V: The Impact of Post-processing on the Tensile, Fatigue and Biological Properties for Medical Implant Applications. *Mater*. (Basel, Switzerland). 13 (2020) 2813. <https://doi.org/10.3390/ma13122813>.
- [16] Hrabec N, Gnäupel-Herold T, Quinn T. Fatigue properties of a titanium alloy (Ti-6Al-4V) fabricated via electron beam melting (EBM): Effects of internal defects and residual stress. *Int J Fatigue* 2017;94:202–10. <https://doi.org/10.1016/j.ijfatigue.2016.04.022>.
- [17] Benzing J, Hrabec N, Quinn T, White R, Rentz R, Ahlfors M. Hot isostatic pressing (HIP) to achieve isotropic microstructure and retain as-built strength in an additive manufacturing titanium alloy (Ti-6Al-4V). *Mater Lett* 2019;257:126690. <https://doi.org/10.1016/j.matlet.2019.126690>.
- [18] Yu H, Li F, Wang Z, Zeng X. Fatigue performances of selective laser melted Ti-6Al-4V alloy: Influence of surface finishing, hot isostatic pressing and heat treatments. *Int J Fatigue* 2019;120:175–83. <https://doi.org/10.1016/j.ijfatigue.2018.11.019>.
- [19] Wu MW, Chen JK, Lin BH, Chiang PH. Improved fatigue endurance ratio of additive manufactured Ti-6Al-4V lattice by hot isostatic pressing. *Mater Des* 2017;134:163–70. <https://doi.org/10.1016/j.matdes.2017.08.048>.
- [20] Seifi M, Salem A, Satko D, Shaffer J, Lewandowski JJ. Defect distribution and microstructure heterogeneity effects on fracture resistance and fatigue behavior of EBM Ti-6Al-4V. *Int J Fatigue* 2017;94:263–87. <https://doi.org/10.1016/j.ijfatigue.2016.06.001>.
- [21] Li P, Warner DH, Pegues JW, Shamsaei N, Roach MD, Phan N, Shamsaei N, Phan N. Investigation of the mechanisms by which hot isostatic pressing improves the fatigue performance of powder bed fused Ti-6Al-4V. *Int J Fatigue* 2019;120(2019) 342–352. <https://doi.org/10.1016/j.ijfatigue.2018.10.015>.
- [22] Moran TP, Carrion PE, Lee S, Shamsaei N, Phan N, Warner DH. Hot Isostatic Pressing for Fatigue Critical Additively Manufactured Ti-6Al-4V. *Materials* (Basel) 2022;15:1–12. <https://doi.org/10.3390/ma15062051>.
- [23] Leyens C, Peters M. Titanium and titanium alloys. Fundamentals and Applications, Wiley-VCH, 2003. https://doi.org/10.1007/978-3-319-69743-7_7.
- [24] Yang J, Yu H, Yin J, Gao M, Wang Z, Zeng X. Formation and control of martensite in Ti-6Al-4V alloy produced by selective laser melting. *Mater Des* 2016;108:308–18. <https://doi.org/10.1016/J.MATDES.2016.06.117>.
- [25] Zafari A, Xia K. High Ductility in a fully martensitic microstructure: a paradox in a Ti alloy produced by selective laser melting. <http://Mc.ManuscriptCentral.Com/Tmrl.6> (2018) 627–633. <https://doi.org/10.1080/21663831.2018.1525773>.
- [26] Liu S, Shin YC. Additive manufacturing of Ti6Al4V alloy: A review. *Mater Des* 2019;164:107552.
- [27] Cao F, Zhang T, Ryder MA, Lados DA. A Review of the Fatigue Properties of Additively Manufactured Ti-6Al-4V. *Jom* 2018;70:349–57. <https://doi.org/10.1007/s11837-017-2728-5>.
- [28] Wycisk E, Siddique S, Herzog D, Walther F, Emmelmann C. Fatigue Performance of laser additive Manufactured Ti-6al-4V in Very high cycle Fatigue regime up to 10⁹ cycles. *Front Mater* 2015;2. <https://doi.org/10.3389/fmats.2015.00072>.
- [29] Wycisk E, Emmelmann C, Siddique S, Walther F. High cycle fatigue (HCF) performance of Ti-6Al-4V alloy processed by selective laser melting. *Adv Mater Res* 2013;816–817:134–9. <https://doi.org/10.4028/www.scientific.net/AMR.816-817.134>.
- [30] Wycisk E, Solbach A, Siddique S, Herzog D, Walther F, Emmelmann C. Effects of defects in laser additive manufactured Ti-6Al-4V on fatigue properties. *Phys Procedia* 2014;56:371–8. <https://doi.org/10.1016/j.phpro.2014.08.120>.
- [31] Rafi HK, Karthik NV, Gong H, Starr TL, Stucker BE. Microstructures and mechanical properties of Ti6Al4V parts fabricated by selective laser melting and electron beam melting. *J Mater Eng Perform* 2013;22:3872–83. <https://doi.org/10.1007/s11665-013-0658-0>.
- [32] Rekedal KD. Investigation of the High-cycle fatigue life of Selective Laser Melted and Hot Isostatically Pressed Ti-6Al-4V, PhD Thesis; 2015.
- [33] Gong H, Rafi K, Gu H, Janaki Ram GD, Starr T, Stucker B. Influence of defects on mechanical properties of Ti-6Al-4V components produced by selective laser melting and electron beam melting. *Mater Des* 2015;86:545–54. <https://doi.org/10.1016/j.matdes.2015.07.147>.
- [34] Xu W, Sun S, Elambasseril J, Liu Q, Brandt M, Qian M. Ti-6Al-4V Additively Manufactured by Selective Laser Melting with Superior Mechanical Properties. *Jom* 2015;67:668–73. <https://doi.org/10.1007/s11837-015-1297-8>.
- [35] Benedetti M, Cazzolli M, Fontanari V, Leoni M. Fatigue limit of Ti6Al4V alloy produced by Selective Laser Sintering. *21ST Eur Conf Fract* 2016;2:3158–67. <https://doi.org/10.1016/j.prostr.2016.06.394>.
- [36] Benedetti M, Torresani E, Leoni M, Fontanari V, Bandini M, Pederzoli C, et al. The effect of post-sintering treatments on the fatigue and biological behavior of Ti-6Al-4V ELI parts made by selective laser melting. *J Mech Behav Biomed Mater* 2017;71:295–306. <https://doi.org/10.1016/j.jmbbm.2017.03.024>.
- [37] Yan X, Yin S, Chen C, Huang C, Bolot R, Lupoi R, et al. Effect of heat treatment on the phase transformation and mechanical properties of Ti6Al4V fabricated by selective laser melting. *Int J Fatigue* 2018;143:1056–71. <https://doi.org/10.1016/j.ijfatigue.2015.12.003>.
- [38] Chastand V, Quaegebeur P, Maia W, Charkaluk E. Comparative study of fatigue properties of Ti-6Al-4V specimens built by electron beam melting (EBM) and selective laser melting (SLM). *Mater Charact* 2018;143:76–81. <https://doi.org/10.1016/J.MATCHAR.2018.03.028>.
- [39] Mertova K, Dzugan J, Roudnicka M. Fatigue properties of SLM-produced Ti6Al4V with various post-processing processes. *IOP Conf Ser Mater Sci Eng* 2018;461. <https://doi.org/10.1088/1757-899X/461/1/012052>.
- [40] Fatemi A, Molaei R, Simsirowig J, Pegues J, Torries B, Shamsaei N, et al. Fatigue behaviour of additive manufactured materials: An overview of some recent experimental studies on Ti-6Al-4V considering various processing and loading direction effects. *Fatigue Fract Eng Mater Struct* 2019;42. <https://doi.org/10.1111/ffe.13000>.
- [41] Smith KN, Waston P, Topper TH. A stress-strain parameter for the fatigue of metals. *J Mech* 1970;15:767.
- [42] Forschungskuratorium Maschinenbau, Analytical strength assessment of components in mechanical engineering FKM-guideline, VDMA Verl., Frankfurt am Main; 2003.
- [43] Li P, Warner DH, Fatemi A, Phan N. Critical assessment of the fatigue performance of additively manufactured Ti-6Al-4V and perspective for future research. *Int J Fatigue* 2016;85:130–43.
- [44] Astm. E8, ASTM E8/EBM standard test methods for tension testing of metallic materials 1. *Annu B ASTM Stand* 2010;4:1–27. <https://doi.org/10.1520/E0008>.
- [45] Boyer RR. Titanium and Its Alloys: Metallurgy, Heat Treatment and Alloy Characteristics. *Encycl Aersp Eng* (2010) 1–12. <https://doi.org/10.1002/9780470686652.eae198>.
- [46] Fan Y, Tian W, Guo Y, Sun Z, Xu J. Relationships among the Microstructure, Mechanical Properties, and Fatigue Behavior in Thin Ti6Al4V. *Adv Mater Sci Eng* 2016;2016:1–9.
- [47] Murakami Y, Beretta S. Small Defects and Inhomogeneities in Fatigue Strength: Experiments, Models and Statistical Implications. *Extremes* 1999;2:123–47.
- [48] Beretta S, Murakami Y. Statistical analysis of defects for fatigue strength prediction and quality control of materials. *Fatigue Fract Eng Mater Struct* 1998;21:1049–65. <https://doi.org/10.1046/j.1460-2695.1998.00104.x>.
- [49] Günther J, Krewerth D, Lippmann T, Leuders S, Tröster T, Weidner A, et al. Fatigue life of additively manufactured Ti-6Al-4V in the very high cycle fatigue regime. *Int J Fatigue* 2017;94:236–45. <https://doi.org/10.1016/j.ijfatigue.2016.05.018>.
- [50] Zhai Y, Galarraga H, Lados DA. Microstructure, static properties, and fatigue crack growth mechanisms in Ti-6Al-4V fabricated by additive manufacturing: LENS and EBM. *Eng Fail Anal* 2016;69:3–14. <https://doi.org/10.1016/j.engfailanal.2016.05.036>.
- [51] Everaerts J, Verlinden B, Wevers M. The influence of the alpha grain size on internal fatigue crack initiation in drawn Ti-6Al-4V wires. *Procedia Struct Integr* 2016;2:1055–62. <https://doi.org/10.1016/j.prostr.2016.06.135>.
- [52] Xue G, Nakamura T, Fujimura N, Takahashi K, Oguma H. Initiation and propagation processes of internal fatigue cracks in β titanium alloy based on fractographic analysis. *Appl Sci* 2021;11:1–17. <https://doi.org/10.3390/app11010131>.
- [53] Furuya Y, Takeuchi E. Gigacycle fatigue properties of Ti-6Al-4V alloy under tensile mean stress. *Mater Sci Eng A* 2014;598:135–40. <https://doi.org/10.1016/j.msea.2014.01.019>.
- [54] Dunne FPE, Rugg D. On the mechanisms of fatigue facet nucleation in titanium alloys. *Fatigue Fract Eng Mater Struct* 2008;31:949–58. <https://doi.org/10.1111/j.1460-2695.2008.01284.x>.
- [55] Everaerts J. Fatigue Crack Initiation and Facet Formation in Ti-6Al-4V Wires; 2017.
- [56] Neal DF, Blenkinsop PA. Internal fatigue origins in α - β titanium alloys. *Acta Metall* 1976;24:59–63. [https://doi.org/10.1016/0001-6160\(76\)90147-4](https://doi.org/10.1016/0001-6160(76)90147-4).
- [57] Bache MR. Processing titanium alloys for optimum fatigue performance. *Int J Fatigue* 1999;21:105–11. [https://doi.org/10.1016/s0142-1123\(99\)00061-4](https://doi.org/10.1016/s0142-1123(99)00061-4).